



Chromatin structure undergoes global and local reorganization during murine dendritic cell development and activation

Daisuke Kurotaki^{a,b,1,2}, Kenta Kikuchi^{a,1}, Kairong Cui^f, Wataru Kawase^b, Keita Saeki^d, Junpei Fukumoto^e, Akira Nishiyama^b, Kisaburo Nagamune^e, Keji Zhao^c, Keiko Ozato^{d,2}, Pedro P. Rocha^{f,g,2}, and Tomohiko Tamura^{b,h,2}

Edited by Kenneth Murphy, Washington University in St. Louis School of Medicine, St. Louis, MO; received April 23, 2022; accepted July 15, 2022

Classical dendritic cells (cDCs) are essential for immune responses and differentiate from hematopoietic stem cells via intermediate progenitors, such as monocyte–DC progenitors (MDPs) and common DC progenitors (CDPs). Upon infection, cDCs are activated and rapidly express host defense-related genes, such as those encoding cytokines and chemokines. Chromatin structures, including nuclear compartments and topologically associating domains (TADs), have been implicated in gene regulation. However, the extent and dynamics of their reorganization during cDC development and activation remain unknown. In this study, we comprehensively determined higher-order chromatin structures by Hi-C in DC progenitors and cDC subpopulations. During cDC differentiation, chromatin activation was initially induced at the MDP stage. Subsequently, a shift from inactive to active nuclear compartments occurred at the cDC gene loci in CDPs, which was followed by increased intra-TAD interactions and loop formation. Mechanistically, the transcription factor IRF8, indispensable for cDC differentiation, mediated chromatin activation and changes into the active compartments in DC progenitors, thereby possibly leading to cDC-specific gene induction. Using an infection model, we found that the chromatin structures of host defense-related gene loci were preestablished in unstimulated cDCs, indicating that the formation of higher-order chromatin structures prior to infection may contribute to the rapid responses to pathogens. Overall, these results suggest that chromatin structure reorganization is closely related to the establishment of cDC-specific gene expression and immune functions. This study advances the fundamental understanding of chromatin reorganization in cDC differentiation and activation.

dendritic cell | hematopoiesis | chromatin structure | transcription factor | infection

Classical dendritic cells (cDCs) are indispensable for inducing innate and acquired immunity (1). These cells recognize pathogen- and damage-associated molecular patterns, stimulating them to produce cytokines, chemokines, and other molecules that activate the innate immune system. Through antigen presentation, cDCs also induce the differentiation of naïve CD4⁺ and CD8⁺ T cells into helper and cytotoxic T cells, respectively. There are two major cDC subpopulations with distinct functions, namely, cDC1s and cDC2s; cDC1s are essential for host defense against intracellular parasitic, viral, and bacterial infections, whereas cDC2s are required for immune responses to extracellular parasites, bacteria, and fungi (2, 3).

The cDCs are derived from bone marrow hematopoietic stem cells via intermediate progenitors (2, 4–7). Progenitor populations expressing FMS-like tyrosine kinase 3 (FLT3) receptor have DC lineage differentiation potential (4, 8). Indeed, the number of cDCs is markedly reduced in mice deficient for FLT3 or its ligand, FLT3L (9, 10). In the mouse hematopoietic system, the most upstream FLT3-expressing progenitor population is lymphoid primed multipotent progenitors (LMPPs). LMPPs differentiate into monocyte–DC progenitors (MDPs), common DC progenitors (CDPs), and pre-cDCs in the bone marrow to generate cDCs (11, 12). The pre-cDCs then migrate into peripheral tissues such as the spleen, where they give rise to cDC1s or cDC2s. Notably, DC lineage specification can occur in upstream hematopoietic progenitors such as LMPPs (11, 13).

Cell differentiation is the process of establishing cell type-specific gene expression patterns, wherein regulation of enhancers by transcription factors plays a critical role. Several transcription factors have been implicated in cDC differentiation. The transcription factors PU.1 and the RUNX1-CBF β complex are required for cDC generation. Mice lacking either PU.1 or CBF β show a severe reduction in FLT3 expression in hematopoietic progenitors, including LMPPs (14, 15). In mice deficient for the transcription factor IRF8, the numbers of CDPs and DCs, particularly cDC1s, are reduced, whereas MDPs accumulate, suggesting that IRF8 is required for the MDP-to-CDP transition (16–21).

Significance

Dendritic cells (DCs), essential for immune responses, originate from bone marrow hematopoietic stem cells via intermediate progenitors. In eukaryotic nuclei, DNA is packaged into 3D chromatin structures that have been implicated in gene regulation. However, the chromatin structure reorganization dynamics during DC differentiation remain unknown. Here, we analyzed 3D chromatin structures in DCs and their progenitors. In genomic regions at DC-specific genes, the 3D chromatin structures were reorganized upon DC differentiation. The transcription factor IRF8 promoted chromatin structure changes in DC progenitors, leading to DC-specific gene induction. Strikingly, the chromatin structures of infection-inducible genes were preestablished in unstimulated DCs. Our findings advance the understanding of DC biology and basic principles of gene regulation for cell differentiation and host defense.

The authors declare no competing interest.

This article is a PNAS Direct Submission.

Copyright © 2022 the Author(s). Published by PNAS. This article is distributed under [Creative Commons Attribution-NonCommercial-NoDerivatives License 4.0 \(CC BY-NC-ND\)](#).

¹D.K. and K.K. contributed equally to this work.

²To whom correspondence may be addressed. Email: kurotaki@kumamoto-u.ac.jp, ozatok@dir6.nichd.nih.gov, pedro.rocha@nih.gov, or tamurat@yokohama-cu.ac.jp.

This article contains supporting information online at <http://www.pnas.org/lookup/suppl/doi:10.1073/pnas.2207009119/-/DCSupplemental>.

Published August 15, 2022.

We recently analyzed the enhancer landscape dynamics during the differentiation of monocytes and cDCs (22). Priming and activation of enhancers associated with genes expressed in monocytes and cDCs are induced by IRF8 in mononuclear phagocyte progenitors such as MDPs. These genes are transcribed in mature monocytes and cDCs but not yet at the progenitor stages (22). These results suggest that a time lag occurs between enhancer establishment and gene expression during cDC differentiation. Additional events, such as remodeling of the chromatin structure, may be involved in this temporal delay (23).

In interphase eukaryotic nuclei, DNA is packaged into higher-order chromatin structures such as nuclear compartments, topologically associating domains (TADs), and promoter–enhancer interactions (24–28). Hi-C, a technique that analyzes the three-dimensional (3D) chromatin architecture of the whole genome, revealed that the genome is subdivided into large megabase-scale A and B compartments (29). The A compartment contains genomic regions with active histone modifications such as histone H3 lysine 27 acetylation (H3K27ac) and transcribing genes, and is localized in the interior nuclear space and nuclear speckles. The B compartment is composed of chromatin with repressive histone modifications and is frequently associated with the nuclear lamina and nucleolus. Loci in the same compartment (that is, A or B) tend to cluster together, while repulsing loci of the opposite compartment. Recent findings suggest that compartments are formed by the assembly of chromatin with similar molecular properties, potentially through mechanisms similar to those of phase separation (30). TADs are locally self-associated chromatin domains and are typically formed via loop extrusion mediated by DNA-bound CTCF and the ring-shaped cohesin complex (31, 32). TADs have been suggested to function as insulators that restrict enhancer–promoter interactions to loci in the same TAD. Therefore, it has been proposed that they play essential roles in gene regulation. However, rapid CTCF or cohesin removal experiments do not necessarily support this view (33, 34). Ubiquitously expressed chromatin proteins, such as cohesin, the mediator complex, and transcription factors, can also mediate enhancer–promoter interactions (25). Although the molecular basis underlying the higher-order chromatin structure formation has been gradually determined, the functions of chromatin structures in gene regulation are still not fully understood.

In cells of the hematopoietic lineage, recent studies have improved the understanding of structural changes in chromatin during T cell and B cell differentiation (35–38); however, knowledge about the chromatin structure organization during cDC differentiation and activation is lacking. In this study, we performed Hi-C on cDC lineage populations, including LMPPs, MDPs, CDPs, cDC1s, and cDC2s. In genomic regions enriched in cDC-specific genes, a shift to the A compartment preceded the rewiring of cDC-specific TADs. We also found that IRF8 promoted the B-to-A compartment shifting in DC progenitors. Moreover, chromatin domains containing infection-inducible gene loci have already been established in unstimulated cDCs. Thus, chromatin structure reorganization is closely related to the establishment of cDC-specific gene expression patterns.

Results

Active Compartment Remodeling Precedes Gene Expression during cDC Differentiation. To understand the changes in higher-order chromatin structures during cDC differentiation, we performed *in situ* Hi-C on LMPPs, MDPs, CDPs, cDC1s, and cDC2s isolated from mice (Fig. 1A, *SI Appendix*, Fig. S1 A and B, and *Dataset S1*) (39). Two independent research groups

identified pre-cDC subpopulations using different surface and intracellular markers in previous studies (40, 41); therefore, the definition of pre-cDCs is not completely consistent. For this reason, pre-cDCs were excluded from our analysis. At the resolution achieved in this study, nuclear compartments and TADs could be observed using our Hi-C data.

Compartments can be identified based on the values of the first principal component (PC1) in principal component analysis of the Hi-C contact maps (Fig. 1B) (29). A and B compartments were defined as genomic regions with positive and negative PC1 values, respectively. Consistent with previous findings, we detected interactions between loci in the same compartment (Fig. 1B) (29, 39). The proportions of the genome in compartments A and B were almost unchanged during cDC differentiation (*SI Appendix*, Fig. S1C). To characterize changes in compartmentalization throughout cDC differentiation, we calculated the PC1 values by dividing the mouse genome into 25-kb bins, followed by *k*-means clustering (Fig. 1C and *Dataset S2*). The PC1 values of the two biological replicates in each population were highly correlated (*SI Appendix*, Fig. S1D). A large portion of the genome was consistently found in the same compartment, with 33.7% labeled as A compartment (cluster [CL]3) and 51.3% labeled as B compartment (CL4 and CL5). We found that 15.0% of the genome underwent compartment switching. CL1 contained regions that changed from B to A (Fig. 1D), whereas regions in CL2 changed from A to B upon differentiation of LMPPs to cDCs. To investigate the temporal relationship between compartment changes, chromatin activation, and gene expression, we performed integrated analysis of Hi-C, H3K27ac chromatin immunoprecipitation sequencing (ChIP-seq), and RNA sequencing (RNA-seq) data. In the CL1 (B-to-A) regions, H3K27ac accumulated from the MDP stage, followed by an increase in PC1 values starting at the CDP stage. The RNA expression of genes associated with CL1 regions was up-regulated when the cells reached the cDC stages (Fig. 1E and *SI Appendix*, Fig. S1E). Opposite results were observed in the CL2 (A-to-B) regions. RNA expression was rapidly down-regulated at the MDP stage. Subsequently, the compartment status gradually changed from A to B, and, finally, H3K27ac enrichment decreased after the CDP stage. Genes in CL1 regions were associated with host defense-related gene ontology (GO) terms, whereas those in CL2 were associated with cell proliferation and differentiation-related GO terms (*SI Appendix*, Fig. S1 F and G and *Dataset S3*). Our data indicate that the activations of enhancers precede the switch in compartmentalization from B to A, leading to the induction of cDC-specific genes.

Rewiring of cDC-Specific TADs Occurs at Later Stages. Next, we analyzed changes in the intra-TAD interaction frequency during cDC differentiation. The Arrowhead algorithm of Juicer software was used to identify TADs (42). Domains identified by this software include typical TADs, sub-TADs, contact domains, and compartment domains (*SI Appendix*, Fig. S2A) (43). By merging TADs across all cell types tested, we identified a total of 7,311 unique TADs. The intra-TAD interaction frequencies of the two biological replicates in each population were highly correlated (*SI Appendix*, Fig. S2B). During cDC differentiation, intra-TAD interactions were established in a cell type-specific manner (Fig. 2A and *Dataset S4*); CL1 TADs were specific to cDC1s, CL2 TADs were specific to cDC2s, CL3 and CL4 TADs were common to cDC1s and cDC2s, and CL5 TADs were common to LMPPs and cDC1s. CL6 and CL7 were TADs that reduced the intradomain interaction frequency during differentiation. For example, CL3 includes

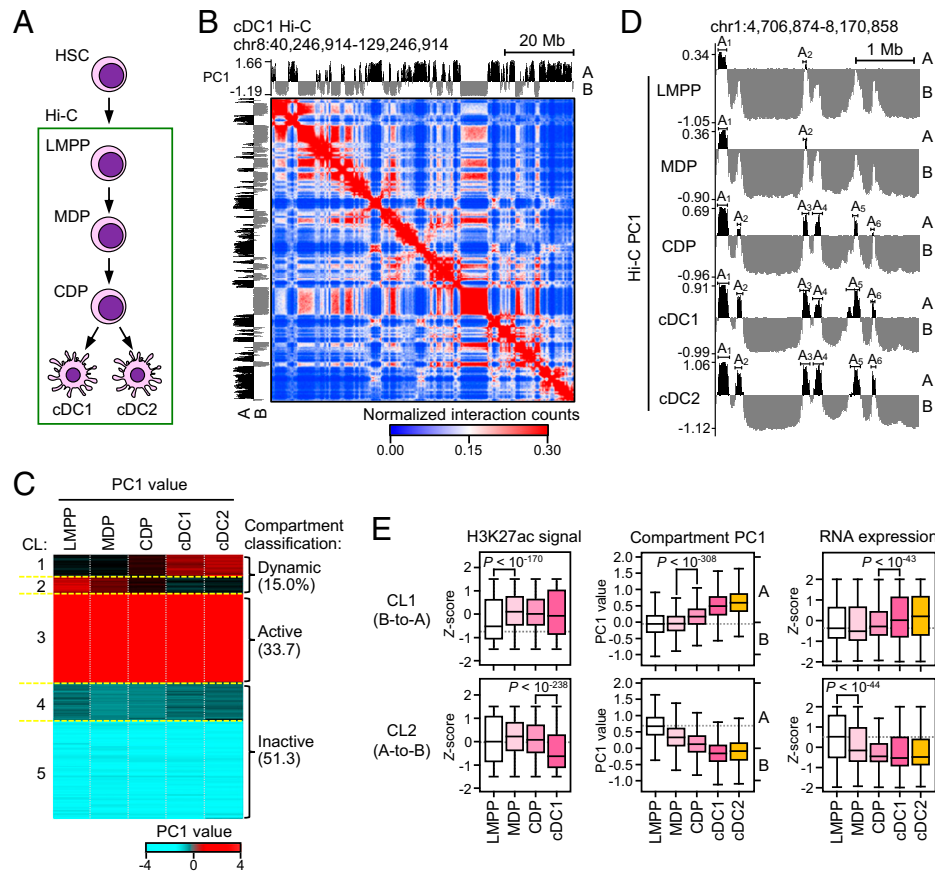


Fig. 1. Nuclear compartment dynamics during cDC differentiation. (A) A differentiation model of cDCs. The green rectangle indicates DC lineage populations subjected to Hi-C analysis. (B) Example of Hi-C contact matrix. The color represents normalized Hi-C interaction counts at indicated genomic regions in chromosome 8 using Homer software. Histograms of PC1 values of the corresponding genomic region are horizontally and vertically shown. Black and gray regions indicate regions in the A and B compartment, respectively. (C) Genome-wide assessment of changes in nuclear compartments during cDC differentiation. The mouse genome was subdivided into 25-kb bins, resulting in 103,531 regions, for PC1 value calculation. The genomic regions were clustered into five using the *k*-means method. Red and blue indicate the A and B compartments, respectively. CL, cluster. (D) University of California, Santa Cruz (UCSC) genome browser image of compartments in LMPPs, MDPs, CDPs, cDC1s, and cDC2s. In this view of chromosome 1, the number of regions in the A compartment increases from two (denoted as A₁ and A₂) in LMPPs to six (denoted as A₁, A₂, A₃, A₄, A₅, and A₆) in cDCs. (E) Kinetics of H3K27ac levels (z score), compartment PC1 values, and gene expression levels (z score) in CL1 or CL2 genomic regions shown by boxplots. Box and center line represent the 25th to 75th percentiles and the median, respectively. Whiskers indicate 1.5-fold of upper and lower interquartile range or the most extreme values. Two-tailed Student's *t* test was performed to calculate statistical significance. In the statistical software we used, 10^{-308} was the lowest *P* value. *P*, *P* value.

the genomic region containing major histocompatibility complex (MHC) class II genes, which are highly expressed in both cDC1s and cDC2s (Fig. 2*B*). Chromatin interactions within the two TADs detected in this region were weak at the progenitor stages, but markedly increased in cDC1s and cDC2s.

We then investigated the relationship between increased intra-TAD interactions, H3K27ac accumulation, and RNA expression in cDC1-specific CL1, cDC2-specific CL2, and cDC-common CL3 (Fig. 2*C*). H3K27ac was slightly enriched in the regions of CL1 and CL3 TADs at the MDP stage. Genes in CL1, CL2, and CL3 TADs were induced at the cDC1, cDC2, and both cDC1 and cDC2 stages, respectively, and were closely linked to increased chromatin interactions within TADs (SI Appendix, Fig. S2*C*). TADs are also characterized by the formation of loops between their boundaries, and stronger loops are associated with TADs of higher insulation. We saw that the cDC-specific TADs formed stronger loops, but there was no significant change in the insulation score at the TAD boundary regions during cDC differentiation (Fig. 2*D* and SI Appendix, Fig. S2*D*). In the genomic regions of CL7 TADs, where chromatin interactions and loop formation diminished during cDC differentiation, H3K27ac enrichment and RNA expression were gradually reduced (Fig. 2*C* and *D*). Similar results were obtained for TADs identified using another

algorithm (Homer) (SI Appendix, Fig. S3). These results indicate that cDC-specific TADs are established at relatively later stages of differentiation, showing a close temporal association with cDC subpopulation-specific gene expression.

A Switch to Compartment A Precedes the Increase in Intra-TAD Interactions at cDC-Specific Gene Loci.

Our results indicate that changes in higher-order chromatin structures are related to the induction of cDC-specific genes. Therefore, we compared the temporal relationship between compartmentalization and TAD formation in chromatin regions containing cDC-specific gene loci. We analyzed RNA-seq data for LMPPs, cDC1s, and cDC2s and identified 1,204 and 1,059 cDC1- and cDC2-specific genes, respectively (SI Appendix, Fig. S1*F*). Approximately 90% of the genomic regions containing these genes were in the A compartment (i.e., CL1 or CL3 shown in Fig. 1*C*) at the cDC stages (Fig. 3*A*). Among them, in regions belonging to CL1 (B-to-A type), H3K27ac levels began increasing in the MDP stage (Fig. 3*B*), which is consistent with our previous results (Fig. 1*E*). This was followed by increases in PC1 values starting from the CDP stage. Subsequently, intra-TAD interactions and TAD loops were enhanced between the CDP and cDC stages, which was correlated with cDC subpopulation-specific gene expression (Fig. 3*B* and SI Appendix, Fig. S4*A*). Likewise, in regions belonging to

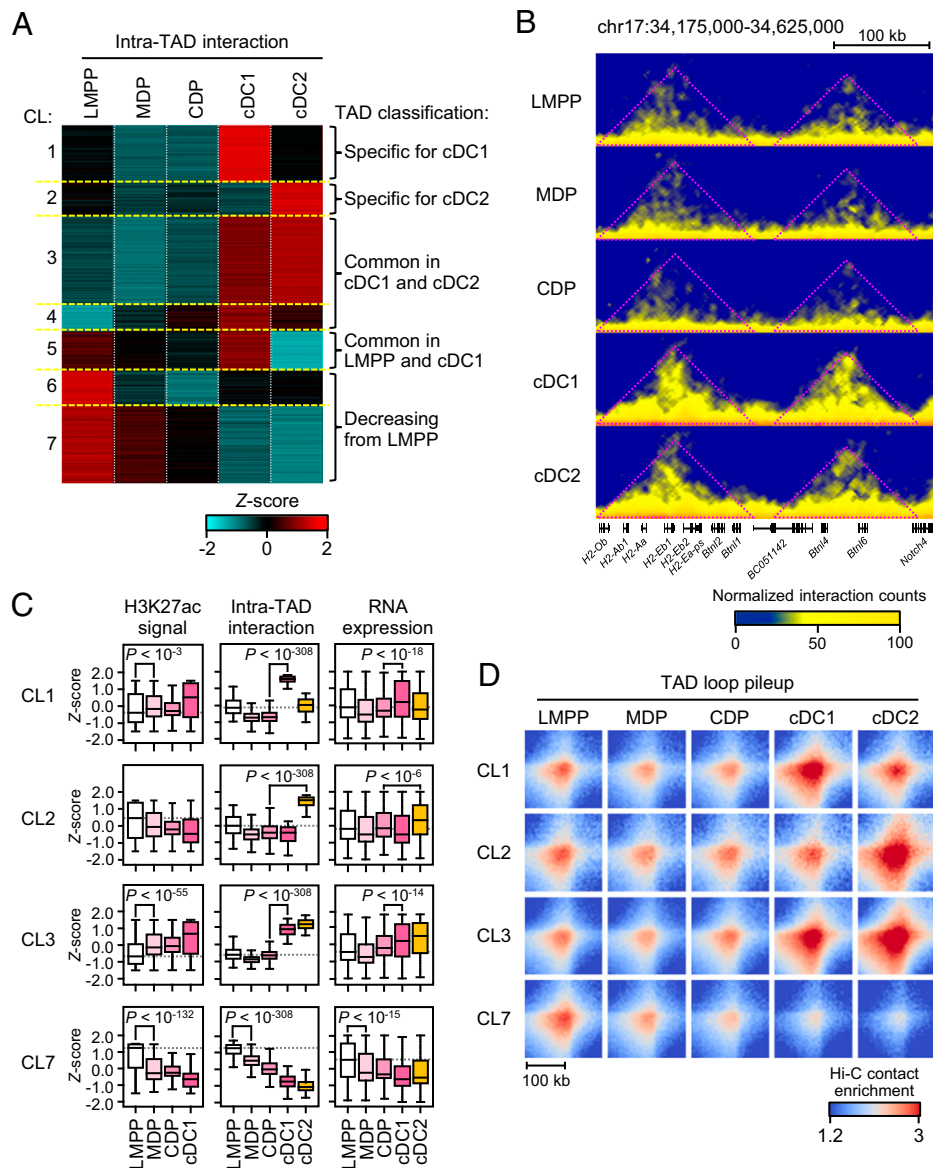


Fig. 2. Dynamics of intra-TAD interactions during cDC differentiation. (A) Kinetics of intra-TAD interaction frequency in cDC differentiation. TADs in each cell population were identified using Juicer software. By merging TADs across all cell types analyzed, we identified 7,311 unique TADs in total. Subsequently, the chromatin interaction frequency within the TADs and its z score were calculated and subdivided into seven clusters using the *k*-means method. (B) Examples of TADs with increased chromatin interactions during cDC differentiation. The Hi-C contact matrix of the MHC class II gene locus on chromosome 17 is shown. (C) Kinetics of H3K27ac levels, frequency of intra-TAD interactions, and RNA expression during cDC differentiation. Boxplots show the z scores. CL1, CL2, CL3, and CL7 TADs, shown in A, were analyzed. Two-tailed Student's *t* test was performed to calculate statistical significance. (D) Pile-up images for TAD loops. The average interaction frequencies between TAD borders of each CL are shown as heatmaps. The signals represent loops formed between TAD borders.

CL3 (A-to-A type), the increase in H3K27ac enrichment was followed by enhanced TAD structures and gene induction (Fig. 3C and *SI Appendix*, Fig. S4A). These results suggest that switching to compartment A occurs first, after which TADs are remodeled in a cell type-specific manner, for cDC gene expression (Fig. 3D).

We also analyzed the genomic regions containing genes whose expression is repressed upon cDC differentiation. Interestingly, these regions were present not only in the B compartments (CL2, CL4, and CL5) but also in the A compartments (CL1 and CL3) at the cDC stages (*SI Appendix*, Fig. S4B), implicating diverse gene silencing mechanisms. Nonetheless, A-to-B compartment shifting occurred concomitantly with diminished TAD structures at 12.2% of repressed gene loci (*SI Appendix*, Fig. S4C). These results indicate that, at least in a fraction of repressed gene loci, changes in chromatin structures might again be involved in regulating gene expression during cDC differentiation.

Transcription Factor IRF8 Promotes H3K27ac Enrichment prior to B-to-A Compartment Change. Our results suggest that switching to the A compartment provides a structural foundation for cDC-specific gene expression. To understand the molecular basis regulating compartmentalization, we focused on genomic regions that changed from B to A during cDC differentiation (Fig. 1C). As described above, chromatin activation, that is, accumulation of H3K27ac, occurred at the MDP stage before the B-to-A compartment change. We previously showed that lineage-specific transcription factors bind to enhancers in mononuclear phagocyte progenitors, leading to enhancer priming and activation (22). Considering that chromatin activation by transcription factors in cDC progenitors may regulate switching to the A compartment, we performed de novo motif analysis in open chromatin regions showing B-to-A compartment changes (Fig. 4A). Although PU.1, CTCF, and RUNX binding motifs were detected in all progenitor stages, PU.1-IRF composite elements were significantly

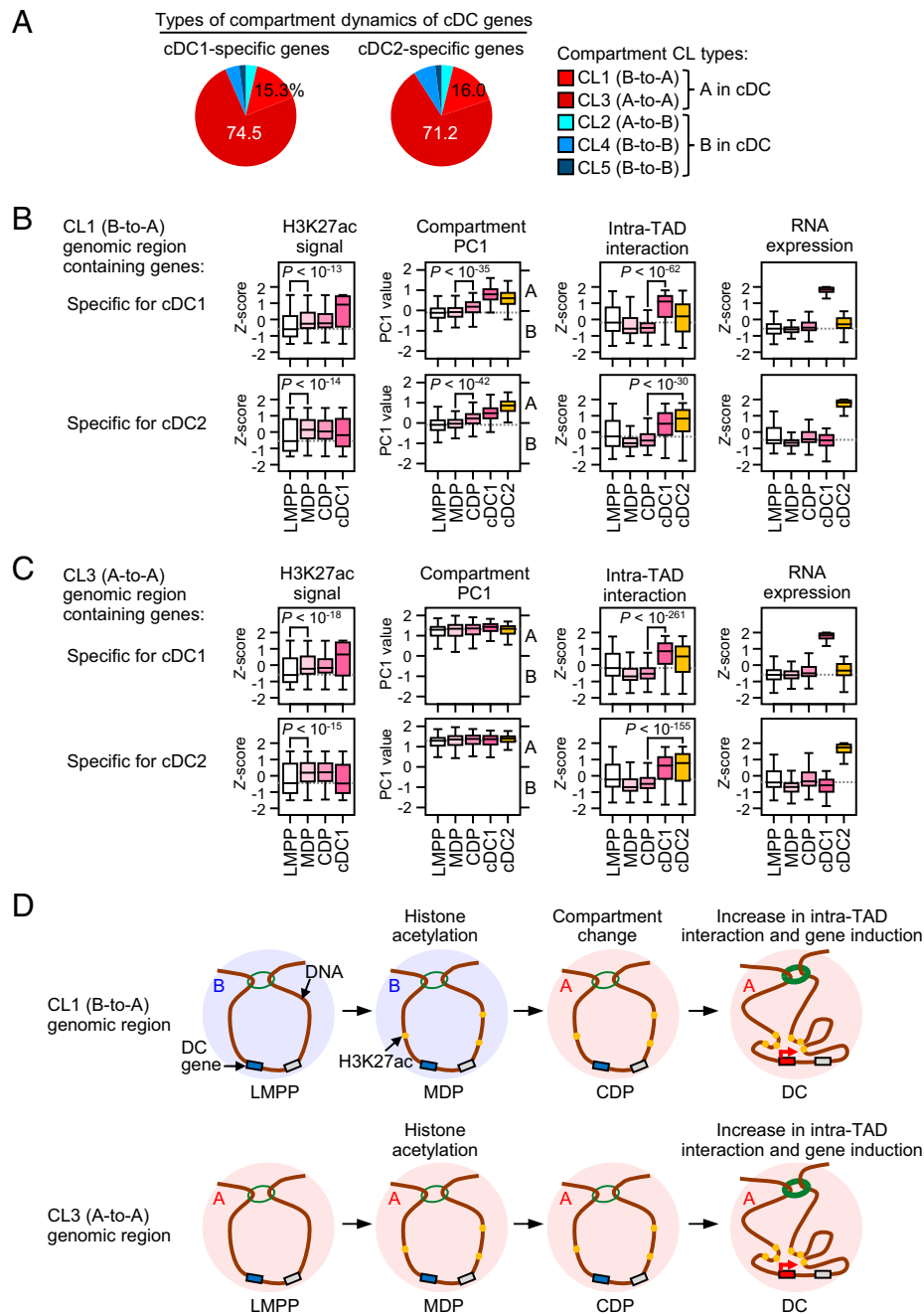


Fig. 3. Chromatin structure reorganization at cDC-specific gene loci. (A) Types of compartment dynamics of cDC-specific gene loci. Compartment dynamics types used here are the CLs shown in Fig. 1C. The cDC1- or cDC2-specific genes were identified from the RNA-seq data. (B and C) Temporal relationship between compartmentalization and TAD formation at genomic regions containing cDC-specific gene loci. CL1 (B) or CL3 (C) compartment regions containing cDC1- or cDC2-specific genes and TADs in these regions were analyzed. Two-tailed Student's *t* test was performed to calculate statistical significance. (D) Schematic models for chromatin structure reorganization at cDC-specific gene loci during cDC differentiation.

enriched in MDPs and CDPs but less frequent in LMPPs. Known motif analysis supported this observation (Fig. 4B). Among the nine IRF family transcription factors, only IRF8 was highly expressed in MDPs and CDPs (Fig. 4C). Notably, in *Irf8*^{-/-} mice, CDPs and cDC1s are severely diminished, whereas MDPs accumulate (17). To investigate whether IRF8 is involved in H3K27ac enrichment before the B-to-A compartment changes during cDC differentiation, we analyzed H3K27ac ChIP-seq data in *Irf8*^{-/-} MDPs. We found that H3K27ac accumulation in genomic regions showing a B-to-A compartment switching and bound by IRF8 in wild-type MDPs was significantly reduced in *Irf8*^{-/-} MDPs (Fig. 4D). Similar results were obtained for open chromatin regions showing the B-to-A compartment changes and

containing known PU.1-IRF motifs (i.e., GGAANNAAA). In contrast, H3K27ac accumulation in B-to-A compartments without the PU.1-IRF binding motif in open chromatin regions was not affected by IRF8 deficiency. These results demonstrate that IRF8 promotes H3K27ac enrichment prior to active compartment formation during cDC differentiation.

IRF8 Induces Switching to A Compartment in DC Progenitors.

To understand the role of IRF8 in active compartment formation during cDC differentiation, we performed Hi-C on *Irf8*^{-/-} MDPs. Two biological replicates for the compartment PC1 values and intra-TAD interaction frequencies in *Irf8*^{-/-} MDPs were highly correlated (SI Appendix, Fig. S5A). Loss of IRF8

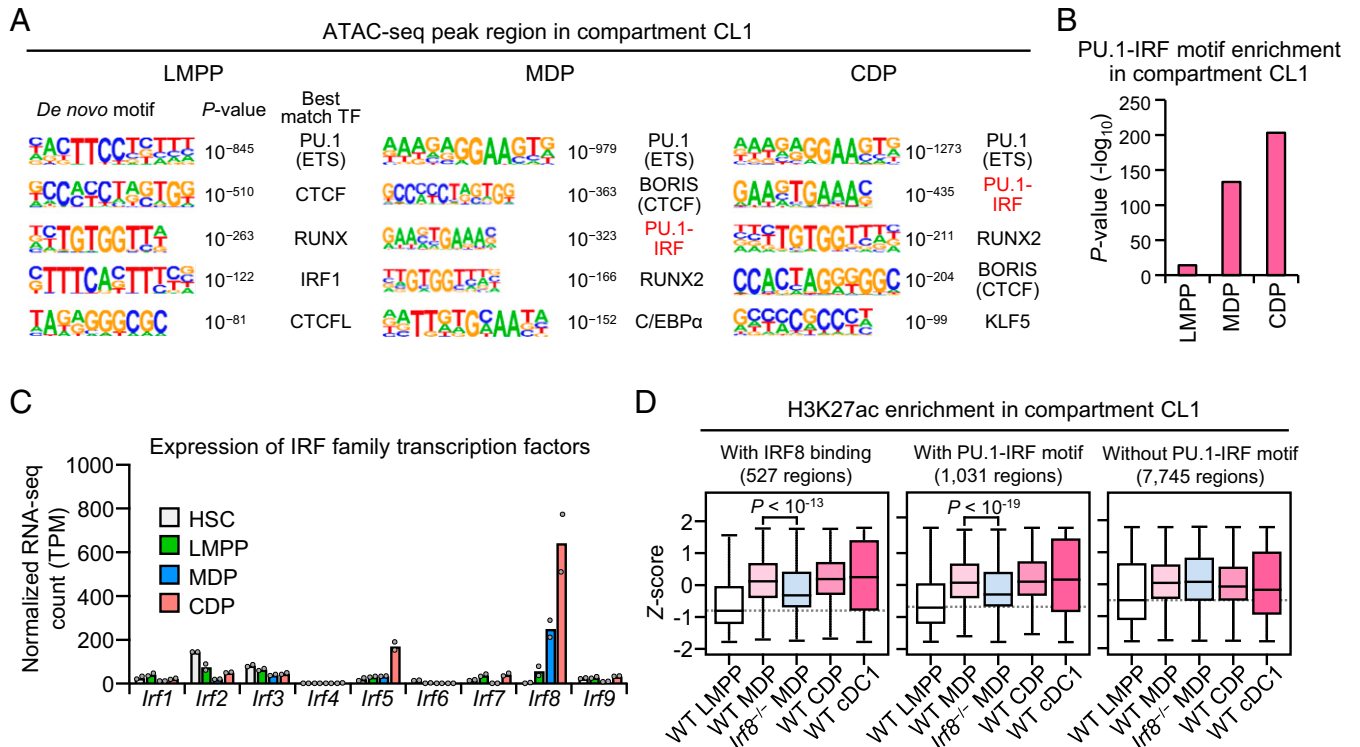


Fig. 4. Identification of transcription factors required for histone acetylation prior to the B-to-A compartment change. (A) De novo motif analysis of open chromatin regions in compartment CL1 defined in Fig. 1C. Open chromatin regions in each progenitor population were identified from assay for transposase-accessible chromatin sequencing (ATAC-seq) data. (B) Known motif analysis for PU.1-IRF binding sites. The “GGAANNGAAA” sequence was searched in the ATAC-seq peak regions in each progenitor population. (C) RNA expression of IRF family transcription factor genes in hematopoietic stem and progenitor populations. Values in the bar graph are the mean \pm SD from two independent experiments. (D) Influence of IRF8 deficiency on H3K27ac accumulation in compartment CL1. ChIP-seq tag densities of H3K27ac in CL1 genomic regions with IRF8 binding (Left) or those with (Middle) or without (Right) known PU.1-IRF motifs (i.e., GGAANNGAAA) in open chromatin regions were analyzed. Two-tailed Student’s *t* test was performed to calculate statistical significance.

affected the PC1 values in 20.2% of the genomic regions in MDPs (Fig. 5A). In *Irf8*^{-/-} MDPs, 10,915 (10.5%) and 10,091 (9.74%) out of the total 103,531 regions displayed significant decrease or increase, respectively, in PC1 values compared to those in the wild-type MDPs, although the number of regions that were judged to have switched from B to A or from A to B was limited (1.75% and 1.46%, respectively; *SI Appendix, Fig. S5B*). Hierarchical clustering revealed that the PC1 value landscape in *Irf8*^{-/-} MDPs was closely related to that in wild-type LMPPs (Fig. 5B). These results suggest that IRF8 is required for compartmentalization changes from LMPPs to MDPs.

To better characterize the direct effect of IRF8 on compartment switching, we performed integrated analysis of the IRF8 ChIP-seq and Hi-C data. In wild-type MDPs, 86.1% and 13.9% of IRF8 binding sites were located in A and B compartments, respectively (*SI Appendix, Fig. S5C*). We found that IRF8 mainly promoted the incorporation into active compartments at its binding sites; among the 4,447 genomic regions showing IRF8 binding in wild-type MDPs, the number of chromatin regions with reduction in PC1 values in *Irf8*^{-/-} MDPs (942 regions) dominated the number of those showing an increase (391 regions; Fig. 5C). For example, IRF8 binds to the *Irf8* gene locus in wild-type MDPs. In these regions, there was a large increase in PC1 values during the transition from LMPPs to MDPs, which did not occur in *Irf8*^{-/-} MDPs (Fig. 5D).

To determine the effects of failure to switch to the A compartment in *Irf8*^{-/-} MDPs on gene expression, we examined the expression of genes associated with the 942 genomic regions where PC1 values were reduced in the absence of IRF8. In wild-type mice, the expression of these genes began increasing at the CDP stage and peaked at the cDC1 stage. We found that

this increase was not observed in the remaining few *Irf8*^{-/-} CDPs (Fig. 5E), which was confirmed by gene set enrichment analysis (GSEA) (Fig. 5F). The effect of IRF8 deficiency on TAD establishment in MDPs appeared to be limited (*SI Appendix, Fig. S5D*). These results indicate that IRF8 promotes the active compartmentalization in DC progenitors, leading to cDC lineage-specific gene expression (Fig. 5G).

Chromatin Structure of Host Defense Genes Is Preestablished in Uninfected cDCs. During infection, cDCs are activated and rapidly express host defense-related genes, such as those encoding cytokines and chemokines (1, 2). For example, during infection by intracellular microbes, such as *Toxoplasma gondii*, cDC1s protect hosts against pathogens by producing proinflammatory cytokines such as IL-12 (44). To characterize how the chromatin structure of defense-related genes is reorganized during differentiation and infection, we performed RNA-seq and Hi-C in splenic cDC1s on day 8 after intraperitoneal injection of *T. gondii* (Dataset S5). The cDC1s from *T. gondii*-infected mice were named Tx cDC1s. Two biological replicates for compartment PC1 values and intra-TAD interactions in Tx cDC1s were highly correlated (*SI Appendix, Fig. S6A*). The expression of 621 and 483 genes was induced and repressed, respectively, in Tx cDC1s, compared to that in control cDC1s (Fig. 6A). As expected, *T. gondii*-induced genes included those for cytokines, such as *Il12b*, and were enriched in genes related to “regulation of defense response” and “regulation of cytokine production” (Fig. 6B and *SI Appendix, Fig. S6B*). We found that genomic regions containing *T. gondii*-inducible gene loci belonged predominantly to the A compartment throughout cDC differentiation (Fig. 6C). Similar to other cDC-specific

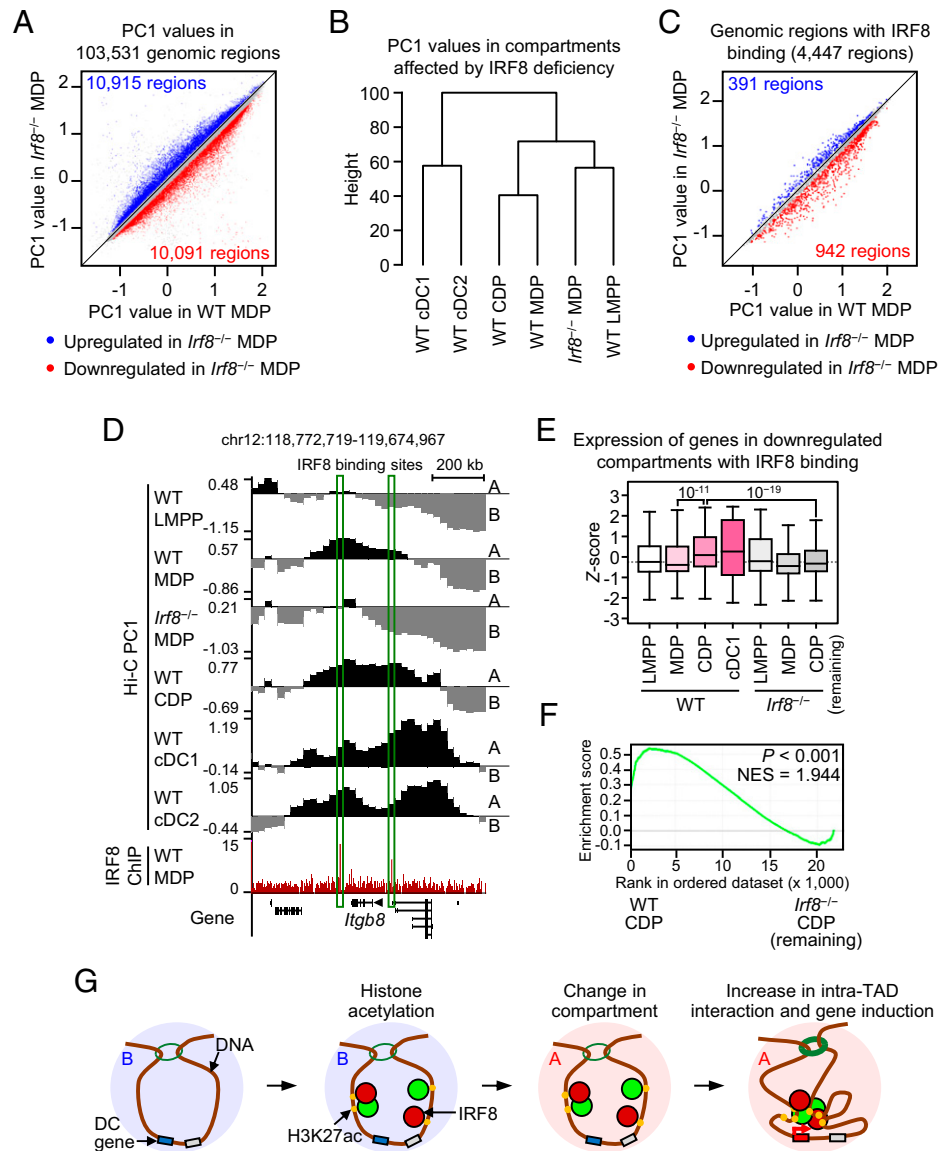


Fig. 5. IRF8 induces switches to compartment A in DC progenitors. (A) Influence of IRF8 deficiency on nuclear compartment formation in MDPs. The mouse genome was subdivided into 25-kb bins, resulting in 103,531 regions as shown in Fig. 1C. PC1 values in each region were calculated in wild-type (WT) MDPs and *Irf8*^{-/-} MDPs. Red and blue dots indicate genomic regions where PC1 values were significantly down-regulated and up-regulated, respectively, in *Irf8*^{-/-} MDPs. We considered a *q* value less than 0.05 as significant. (B) Hierarchical clustering analysis of regions where PC1 values were significantly altered by the absence of IRF8 in MDPs. (C) Comparison of PC1 values at IRF8 binding sites between WT MDPs and *Irf8*^{-/-} MDPs. IRF8 binding sites were identified from IRF8 ChIP-seq data in WT MDPs. (D) Example of compartment change at IRF8 binding sites near the *Itgb8* gene. (E) RNA expression of genes included in the 942 IRF8-bound genomic regions where PC1 values were significantly down-regulated. Two-tailed Student's *t* test was performed to calculate statistical significance. (F) GSEA comparing WT CDPs with *Irf8*^{-/-} CDPs for genes included in the 942 genomic regions analyzed in E. (G) Schematic model of the role of IRF8 in compartment formation during cDC differentiation.

genes (Fig. 3 B and C), genomic regions containing these genes began to show increased H3K27ac levels from the MDP stage. Interestingly, intra-TAD interactions and TAD loop formation at these genomic regions were already established in the uninfected cDC1s and were not reinforced by *T. gondii* infection (Fig. 6C and SI Appendix, Fig. S6C). Notably, the chromatin structures at genomic regions containing genes repressed in Tx cDC1s showed similar kinetics (SI Appendix, Fig. S6D).

To investigate whether the chromatin structure of genes induced by other stimuli in DCs was also preestablished before infection, we performed additional analyses on other stimulus-responsive gene sets in DCs retrieved from the Molecular Signatures Database (45) (SI Appendix, Fig. S6E and Dataset S6). We found that, regardless of the type of stimulus, intra-TAD interactions at genomic regions containing induced genes were enhanced in steady-state cDC1s and/or cDC2s. These results

suggest that higher-order chromatin structures of infection- and stimulus-responsive genes are preestablished in steady-state cDCs before stimulation (Fig. 6D).

Discussion

In this study, we determined the remodeling dynamics of higher-order chromatin structures during cDC differentiation and activation in vivo. Upon cDC differentiation, the composition of the active compartment changes, followed by the rewiring of intra-TAD interactions, causing higher-order chromatin structures to induce cDC-specific genes. One of the molecules responsible for compartment changes is the transcription factor IRF8, which promotes the formation of active compartments in DC progenitors. Furthermore, we showed that higher-order chromatin structures containing host defense-related gene loci

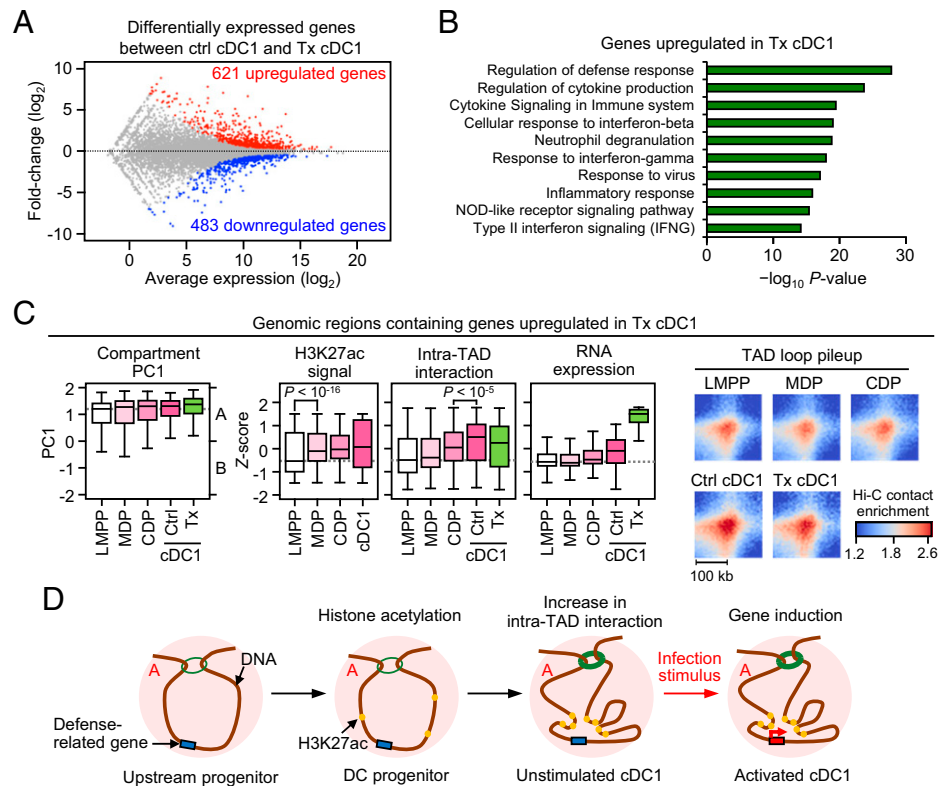


Fig. 6. Chromatin structure reorganization at host defense-related genes in cDC1s. (A) Differentially expressed genes between cDC1s from uninfected mice (control [ctrl] cDC1) and those from *T. gondii*-infected mice (Tx cDC1). Red and blue dots indicate significantly up-regulated and down-regulated genes, respectively, in Tx cDC1s. (B) GO analysis of the genes up-regulated in Tx cDC1s. (C) Kinetics of chromatin structure reorganization at host defense-related gene loci. (Left) The mouse genome was subdivided into 25-kb bins, resulting in 103,531 regions as shown in Fig. 1C. Among these regions, those containing the genes up-regulated in Tx cDC1s were selected. TADs in these regions were then identified. Compartment PC1 values of the genomic regions and the z scores for H3K27ac signals, chromatin interactions within TADs, and RNA expression of up-regulated genes are shown as box plots. Two-tailed Student's *t* test was performed to calculate statistical significance. (Right) The average frequencies of interactions between the TAD borders, that is, TAD loops, are shown as heatmaps. (D) Schematic model of chromatin structure reorganization at host defense-related gene loci during cDC differentiation and activation.

are already preestablished in uninfected cDCs. These results advance the understanding of mechanisms regulating gene expression during immune cell differentiation and activation.

We demonstrated the order in which different levels of chromatin structures were established during cDC differentiation. Previous studies suggested that changes in compartmentalization and increased chromatin interactions within TADs precede or occur simultaneously with gene expression during cell differentiation and reprogramming (35, 46–48). In addition, TAD boundaries were reported to be altered in genomic regions where compartment changes occur during cell differentiation (35, 46, 47). However, the precise timing of active compartment formation and TAD establishment during cell differentiation remains unclear. In this study, we found that the formation of higher-order chromatin structures containing cDC-specific gene loci exhibited two main patterns: the genomic regions showing B-to-A compartment change from the CDP stage and the regions that persistently localize in the A compartment throughout cDC differentiation. The TADs present in these A compartments show a substantial increase in chromatin interactions and loop formation at later stages than in CDPs, eventually resulting in cDC-specific gene induction. Approximately 90% of cDC-specific gene loci are present in the A compartments, with increased intra-TAD interactions at the cDC stages, suggesting that active compartment formation and subsequent TAD establishment are essential for gene expression in cDCs.

Although IRF8 is an indispensable transcription factor for the differentiation of DCs, especially cDC1s (49), its role in higher-order chromatin structure establishment had not been

reported. We found that IRF8 induced active H3K27ac accumulation at its binding sites during cDC differentiation and induces some of these cDC-specific regions to switch to compartment A. However, the molecular mechanisms underlying this compartmentalization change remain unknown. It has been proposed that phase separation is involved in the formation of compartments (30, 43). Previous studies showed that histone acetylation induces phase separation of chromatin in the presence of bromodomain proteins, such as BRD4, thereby contributing to the formation of active compartments (50, 51). BRD4 itself is also involved in the phase separation process and chromatin conformation changes (52, 53). IRF8 can form a protein complex with BRD4 (54). Thus, histone acetylation and BRD4 accumulation may be required for the compartment switching induced by IRF8. To clarify the molecular mechanism underlying IRF8-mediated compartmentalization, future investigation of IRF8-interacting proteins and their involvement in phase separation are needed.

The molecular basis of the increase in intra-TAD chromatin interactions and loop formation surrounding cDC-specific gene loci at the final stages of cDC differentiation is also unclear. Intra-TAD interactions include promoter–enhancer interactions that can be formed by structural proteins, such as the cohesin complex and protein–protein interactions mediated by transcription factors and chromatin regulators (25). Indeed, CIITA, which is important for the regulation of MHC class II gene expression, promotes enhancer–promoter interactions at the MHC class II gene locus by bridging various transcription factors (55). Previous studies showed that histone acetylation

also contributes to the formation of promoter–enhancer interactions (56). As enhanced intra-TAD interactions are accompanied by H3K27ac enrichment in cDC differentiation, histone acetylation may also be involved in increasing intra-TAD interactions. Furthermore, TADs are established in a cDC1- or cDC2-specific manner (Fig. 2A), suggesting that factors specific to the cDC subpopulation regulate the increase in intra-TAD interactions.

We also revealed the stage of hematopoietic cell differentiation in which higher-order chromatin structures of infection-inducible gene loci are established. Genomic regions containing *T. gondii* infection-inducible genes were predominantly present in the A compartments from the LMPP stage, followed by enhanced intra-TAD interactions in uninfected cDC1s, despite these genes being barely expressed until infection occurred. Based on these observations, we hypothesize that the formation of higher-order chromatin structures in immune cells prior to infection contributes to their rapid response to pathogens. Indeed, CTCF or cohesin depletion disrupts TAD organization, leading to impairments in inflammatory gene induction by lipopolysaccharides in macrophages (57–59). Previous studies showed that, in *Drosophila melanogaster* embryogenesis and in a human cell line, chromatin interactions at many gene loci are formed prior to the induction of gene expression and are associated with paused RNA polymerase II (60, 61). In steady-state macrophages, RNA polymerase is stalled at the promoters of inflammatory genes, such as *Tnf* (62). In addition, it has been reported that bivalent chromatin domains marked by H3K4me3 and H3K27me3 are formed at some inflammation-inducible genes such as *Bmp2* in macrophages before stimulation (63, 64). Thus, we envisage that the poised chromatin state with RNA polymerase II pausing and bivalent chromatin marks may be involved in the repression of genes at which higher-order chromatin structures are already established. Understanding the functional role of preformed higher-order chromatin structures would help us understand the basic principles underlying the induction of infection-inducible genes in immune cells.

Materials and Methods

Detailed descriptions for all procedures are available in *SI Appendix*.

Mice. Male wild-type and *Irf8*^{−/−} mice 8 wk to 10 wk old in a C57BL/6 background were used. All animal experiments were performed in accordance with the specifications of the Association for Assessment and Accreditation of Laboratory Animal Care in the United States and Guidelines for Proper Conduct of Animal Experiments (Science Council of Japan) in Japan. Animal procedures were performed according to animal study protocols (ASP# 17-044 and 20-144 in NIH, F-A-17-018 in Yokohama City University, and 119050 in National Institute of Infectious Diseases in Japan).

***T. gondii* Infection.** *T. gondii* (Pru strain) parasites were maintained using human foreskin fibroblasts as previously described (65); 10⁴ *T. gondii* tachyzoites were resuspended in phosphate-buffered saline and intraperitoneally inoculated into mice.

Cell Isolation. Bone marrow and spleen cells were obtained by flushing the femur and tibia and with Liberase and DNase I (Roche) treatment, respectively (11). To isolate bone marrow progenitors, lineage marker negative (Lin[−]) cells were enriched using Lineage Cell Depletion Kit (Miltenyi Biotech). Lin[−] cells were further stained with fluorochrome-labeled antibodies, followed by fluorescence-activated cell sorting (FACS) with FACSARIA II. Because FACS separation of cDCs caused severe damage to the chromatin, cDC1s and cDC2s were isolated using magnetic beads using CD8⁺ and CD4⁺ Dendritic Cell Isolation Kits,

respectively. The purity of the cell populations using FACS and magnetic beads was >99% and >95%, respectively.

Hi-C. Hi-C was performed as previously described (66). Briefly, isolated cells were fixed with formaldehyde. The nuclei were isolated with lysis buffer and digested with DpnII (NEB) at 37 °C. The DNA overhangs were filled with biotin-labeled deoxyadenosine triphosphate (Thermo) using Klenow DNA polymerase (NEB). Samples were treated with T4 DNA Ligase (NEB) at 16 °C. The ligated DNA was purified using phenol-chloroform-isoamyl alcohol (Sigma) and sheared using Covaris ME220. Streptavidin C1 beads (Thermo) were used to enrich the biotin-labeled DNA fragments. To generate Hi-C libraries, KAPA hyper prep kit was used. Each Hi-C library was sequenced on Illumina HiSeq or NextSeq 500.

Mapping Hi-C Reads. Initial Hi-C data processing was followed by the instruction of Homer software website (<http://homer.ucsd.edu/homer/interactions/HiCtagDirectory.html>).

Identification of Nuclear Compartments. To identify the nuclear compartment (29), primary component analysis of the Hi-C data was performed using the Homer runHiCpca.pl module.

Identification of TADs. TADs were identified using the Juicer Arrowhead algorithm (42). TADs in LMPPs, MDPs, CDPs, cDC1s, and cDC2s were merged into a common set of unique TADs using the Homer merge2Dbed.pl module.

Data, Materials, and Software Availability. RNA-seq data on *T. gondii* infection experiments and Hi-C data have been deposited in the DNA Data Bank of Japan (DDBJ) and are publicly available as of the date of publication (accession code [PRJDB13154](https://www.ncbi.nlm.nih.gov/nuccore/PRJDB13154)) (67). Other sequencing data were previously published and are available at the DDBJ (accession code [PRJDB3411](https://www.ncbi.nlm.nih.gov/nuccore/PRJDB3411)) (68) and Gene Expression Omnibus (accession code [GSE149762](https://www.ncbi.nlm.nih.gov/geo/query/acc.cgi?acc=GSE149762)) (69).

ACKNOWLEDGMENTS. We thank Dr. Koichi Murakami and Mr. Masahiro Yoshinari at Yokohama City University, Dr. Yutaka Suzuki and Dr. Shinichi Morishita at The University of Tokyo, and Dr. Tiyun Wu, Dr. Anup Dey, Dr. Vishal Nehru, and Dr. Eri Hosogane at NIH for their help with the experiments and analyses. This work was supported by Grants-in-Aid for Scientific Research from the Japan Society for the Promotion of Science (JSPS)/Ministry of Education, Culture, Sports, Science and Technology (MEXT) (Grants JP19H03691, JP17KK0171, and JP16H06279 [Platform for Advanced Genome Science] to D.K., JP21K20778 to K.K., and JP21H02954 to T.T.); Japanese Society of Hematology Research Grants (to D.K. and T.T.); research grants from the Waksman Foundation of Japan, the Novartis Foundation in Japan for the Promotion of Science, the Chemo-Sero-Therapeutic Research Institute, the Tokyo Biochemical Research Foundation, and the Hoyu Science Foundation (to D.K.); Gene Grant from NIPPON Genetics Co, Ltd (to K.K.); Uehara Memorial Foundation Research Grant (to T.T.); Eunice Kennedy Shriver National Institute of Child Health and Human Development (NICHD) Intramural Programs (to K.O. and P.P.R.), and National Heart, Lung, and Blood Institute (NHLBI) Intramural Programs (to K.Z.). This study was also supported by the Kumamoto University Hospital Research Revitalization Project, the JSPS Core-to-Core Program A of Advanced Research Networks at Kumamoto University, and MEXT Promotion of Distinctive Joint Research Center Program (Grants JPMXP0618217493 and JPMXP0622717006) at the Advanced Medical Research Center, Yokohama City University.

Author affiliations: ^aLaboratory of Chromatin Organization in Immune Cell Development, International Research Center for Medical Sciences, Kumamoto University, Kumamoto 860-0811, Japan; ^bDepartment of Immunology, Yokohama City University Graduate School of Medicine, Yokohama 236-0004, Japan; ^cLaboratory of Epigenome Biology, Systems Biology Center, National Heart, Lung, and Blood Institute, NIH, Bethesda, MD 20814; ^dProgram in Genomics of Differentiation, Eunice Kennedy Shriver National Institute of Child Health and Human Development, NIH, Bethesda, MD 20892; ^eDepartment of Parasitology, National Institute of Infectious Diseases, Tokyo 162-8640, Japan; ^fUnit on Genome Structure and Regulation, Eunice Kennedy Shriver National Institute of Child Health and Human Development, NIH, Bethesda, MD 20892; ^gNational Cancer Institute, NIH, Bethesda, MD 20892; and ^hAdvanced Medical Research Center, Yokohama City University, Yokohama 236-0004, Japan

Author contributions: D.K., P.P.R., and T.T. designed research; D.K., K.C., W.K., K.S., J.F., A.N., and K.N. performed research; D.K., K.K., and T.T. analyzed data; D.K., K.K., K.O., P.P.R., and T.T. wrote the paper; D.K. and T.T. supervised the project; K.N., K.Z., K.O., and P.P.R. provided key materials; and K.Z., K.O., and P.P.R. provided critical suggestions.

1. R. M. Steinman, Decisions about dendritic cells: Past, present, and future. *Annu. Rev. Immunol.* **30**, 1–22 (2012).
2. D. A. Anderson 3rd, C. A. Dutertre, F. Ginhoux, K. M. Murphy, Genetic models of human and mouse dendritic cell development and function. *Nat. Rev. Immunol.* **21**, 101–115 (2021).
3. A. Mildner, S. Jung, Development and function of dendritic cell subsets. *Immunity* **40**, 642–656 (2014).
4. K. Shortman, S. H. Naik, Steady-state and inflammatory dendritic-cell development. *Nat. Rev. Immunol.* **7**, 19–30 (2007).
5. M. Guilliams *et al.*, Dendritic cells, monocytes and macrophages: A unified nomenclature based on ontogeny. *Nat. Rev. Immunol.* **14**, 571–578 (2014).
6. K. Liu, M. C. Nussenzweig, Origin and development of dendritic cells. *Immunol. Rev.* **234**, 45–54 (2010).
7. F. Geissmann, S. Gordon, D. A. Hume, A. M. Mowat, G. J. Randolph, Unravelling mononuclear phagocyte heterogeneity. *Nat. Rev. Immunol.* **10**, 453–460 (2010).
8. A. D'Amico, L. Wu, The early progenitors of mouse dendritic cells and plasmacytoid dendritic cells are within the bone marrow hemopoietic precursors expressing Flt3. *J. Exp. Med.* **198**, 293–303 (2003).
9. H. J. McKenna *et al.*, Mice lacking flt3 ligand have deficient hematopoiesis affecting hematopoietic progenitor cells, dendritic cells, and natural killer cells. *Blood* **95**, 3489–3497 (2000).
10. C. Waskow *et al.*, The receptor tyrosine kinase Flt3 is required for dendritic cell development in peripheral lymphoid tissues. *Nat. Immunol.* **9**, 676–683 (2008).
11. D. Kurotaki *et al.*, Epigenetic control of early dendritic cell lineage specification by the transcription factor IRF8 in mice. *Blood* **133**, 1803–1813 (2019).
12. T. Ohteki, S. Kawamura, N. Onai, Commitment to dendritic cells and monocytes. *Int. Immunol.* **33**, 815–819 (2021).
13. S. H. Naik *et al.*, Diverse and heritable lineage imprinting of early haematopoietic progenitors. *Nature* **496**, 229–232 (2013).
14. S. Carotta *et al.*, The transcription factor PU.1 controls dendritic cell development and Flt3 cytokine receptor expression in a dose-dependent manner. *Immunity* **32**, 628–641 (2010).
15. A. T. Satpathy *et al.*, Runx1 and Cbfb regulate the development of Flt3⁺ dendritic cell progenitors and restrict myeloproliferative disorder. *Blood* **123**, 2968–2977 (2014).
16. J. Aliberti *et al.*, Essential role for ICSBP in the in vivo development of murine CD8alpha⁺ dendritic cells. *Blood* **101**, 305–310 (2003).
17. D. Kurotaki *et al.*, IRF8 inhibits C/EBPα activity to restrain mononuclear phagocyte progenitors from differentiating into neutrophils. *Nat. Commun.* **5**, 4978 (2014).
18. A. M. Becker *et al.*, IRF8 extinguishes neutrophil production and promotes dendritic cell lineage commitment in both myeloid and lymphoid mouse progenitors. *Blood* **119**, 2003–2012 (2012).
19. K. Murakami *et al.*, A RUNX-CBFB-driven enhancer directs the *Irf8* dose-dependent lineage choice between DCs and monocytes. *Nat. Immunol.* **22**, 301–311 (2021).
20. D. Sichien *et al.*, IRF8 transcription factor controls survival and function of terminally differentiated conventional and plasmacytoid dendritic cells, respectively. *Immunity* **45**, 626–640 (2016).
21. S. Kim *et al.*, High amount of transcription factor IRF8 engages AP1-IRF composite elements in enhancers to direct type 1 conventional dendritic cell identity. *Immunity* **54**, 1622 (2021).
22. D. Kurotaki *et al.*, Transcription factor IRF8 governs enhancer landscape dynamics in mononuclear phagocyte progenitors. *Cell Rep.* **22**, 2628–2641 (2018).
23. E. E. M. Furlong, M. Levine, Developmental enhancers and chromosome topology. *Science* **361**, 1341–1345 (2018).
24. A. S. Hansen, C. Cattoglio, X. Darzacq, R. Tjian, Recent evidence that TADs and chromatin loops are dynamic structures. *Nucleus* **9**, 20–32 (2018).
25. R. Stadhouders, G. J. Filion, T. Graf, Transcription factors and 3D genome conformation in cell-fate decisions. *Nature* **569**, 345–354 (2019).
26. J. Dekker, L. Mirny, The 3D genome as moderator of chromosomal communication. *Cell* **164**, 1110–1121 (2016).
27. T. Misteli, The self-organizing genome: Principles of genome architecture and function. *Cell* **183**, 28–45 (2020).
28. T. Sexton, G. Cavalli, The role of chromosome domains in shaping the functional genome. *Cell* **160**, 1049–1059 (2015).
29. E. Lieberman-Aiden *et al.*, Comprehensive mapping of long-range interactions reveals folding principles of the human genome. *Science* **326**, 289–293 (2009).
30. E. M. Hildebrand, J. Dekker, Mechanisms and functions of chromosome compartmentalization. *Trends Biochem. Sci.* **45**, 385–396 (2020).
31. M. Merkschlager, E. P. Nora, CTCF and cohesin in genome folding and transcriptional gene regulation. *Annu. Rev. Genomics Hum. Genet.* **17**, 17–43 (2016).
32. L. Vian *et al.*, The energetics and physiological impact of cohesin extrusion. *Cell* **173**, 1165–1178.e20 (2018).
33. S. S. P. Rao *et al.*, Cohesin loss eliminates all loop domains. *Cell* **171**, 305–320.e24 (2017).
34. E. P. Nora *et al.*, Targeted degradation of CTCF decouples local insulation of chromosome domains from genomic compartmentalization. *Cell* **169**, 930–944.e22 (2017).
35. G. Hu *et al.*, Transformation of accessible chromatin and 3D nucleome underlies lineage commitment of early T cells. *Immunity* **48**, 227–242.e8 (2018).
36. R. Vilarasa-Blasi *et al.*, Dynamics of genome architecture and chromatin function during human B cell differentiation and neoplastic transformation. *Nat. Commun.* **12**, 651 (2021).
37. T. M. Johanson *et al.*, Transcription-factor-mediated supervision of global genome architecture maintains B cell identity. *Nat. Immunol.* **19**, 1257–1264 (2018).
38. J. M. R. Pongubala, C. Murre, Spatial organization of chromatin: Transcriptional control of adaptive immune cell development. *Front. Immunol.* **12**, 633825 (2021).
39. S. S. Rao *et al.*, A 3D map of the human genome at kilobase resolution reveals principles of chromatin looping. *Cell* **159**, 1665–1680 (2014).
40. A. Schlitzer *et al.*, Identification of cDC1- and cDC2-committed DC progenitors reveals early lineage priming at the common DC progenitor stage in the bone marrow. *Nat. Immunol.* **16**, 718–728 (2015).
41. G. E. Grajales-Reyes *et al.*, Batf3 maintains autoactivation of *Irf8* for commitment of a CD8α⁺ conventional DC clonogenic progenitor. *Nat. Immunol.* **16**, 708–717 (2015).
42. N. C. Durand *et al.*, Juicer provides a one-click system for analyzing loop-resolution Hi-C experiments. *Cell Syst.* **3**, 95–98 (2016).
43. A. M. Oudelaar, D. R. Higgs, The relationship between genome structure and function. *Nat. Rev. Genet.* **22**, 154–168 (2021).
44. M. Mashayekhi *et al.*, CD8α⁺ dendritic cells are the critical source of interleukin-12 that controls acute infection by *Toxoplasma gondii* tachyzoites. *Immunity* **35**, 249–259 (2011).
45. A. Liberzon *et al.*, The Molecular Signatures Database (MSigDB) hallmark gene set collection. *Cell Syst.* **1**, 417–425 (2015).
46. J. R. Dixon *et al.*, Chromatin architecture reorganization during stem cell differentiation. *Nature* **518**, 331–336 (2015).
47. H. Miura *et al.*, Single-cell DNA replication profiling identifies spatiotemporal developmental dynamics of chromosome organization. *Nat. Genet.* **51**, 1356–1368 (2019).
48. R. Stadhouders *et al.*, Transcription factors orchestrate dynamic interplay between genome topology and gene regulation during cell reprogramming. *Nat. Genet.* **50**, 238–249 (2018).
49. D. Kurotaki, T. Tamura, Transcriptional and epigenetic regulation of innate immune cell development by the transcription factor, interferon regulatory factor-8. *J. Interferon Cytokine Res.* **36**, 433–441 (2016).
50. B. A. Gibson *et al.*, Organization of chromatin by intrinsic and regulated phase separation. *Cell* **179**, 470–484.e21 (2019).
51. C. D. Rosencrance *et al.*, Chromatin hyperacetylation impacts chromosome folding by forming a nuclear subcompartment. *Mol. Cell* **78**, 112–126.e12 (2020).
52. X. Han *et al.*, Roles of the BRD4 short isoform in phase separation and active gene transcription. *Nat. Struct. Mol. Biol.* **27**, 333–341 (2020).
53. K. L. Cheung, C. Kim, M. M. Zhou, The functions of BET proteins in gene transcription of biology and diseases. *Front. Mol. Biosci.* **8**, 728777 (2021).
54. X. Dong *et al.*, Brd4 regulates NLR4 inflammasome activation by facilitating IRF8-mediated transcription of *Naip3*. *J. Cell Biol.* **220**, e202005148 (2021).
55. K. L. Wright, J. P. Ting, Epigenetic regulation of MHC-II and *CIITA* genes. *Trends Immunol.* **27**, 405–412 (2006).
56. S. Sungalee *et al.*, Histone acetylation dynamics modulates chromatin conformation and allele-specific interactions at oncogenic loci. *Nat. Genet.* **53**, 650–662 (2021).
57. T. Nikolic *et al.*, The DNA-binding factor Ctcf critically controls gene expression in macrophages. *Cell. Mol. Immunol.* **11**, 58–70 (2014).
58. G. Stik *et al.*, CTCF is dispensable for immune cell transdifferentiation but facilitates an acute inflammatory response. *Nat. Genet.* **52**, 655–661 (2020).
59. S. Cuartero *et al.*, Control of inducible gene expression links cohesin to hematopoietic progenitor self-renewal and differentiation. *Nat. Immunol.* **19**, 932–941 (2018).
60. F. Jin *et al.*, A high-resolution map of the three-dimensional chromatin interactome in human cells. *Nature* **503**, 290–294 (2013).
61. Y. Ghavi-Helm *et al.*, Enhancer loops appear stable during development and are associated with paused polymerase. *Nature* **512**, 96–100 (2014).
62. K. Adelman *et al.*, Immediate mediators of the inflammatory response are poised for gene activation through RNA polymerase II stalling. *Proc. Natl. Acad. Sci. U.S.A.* **106**, 18207–18212 (2009).
63. B. E. Bernstein *et al.*, A bivalent chromatin structure marks key developmental genes in embryonic stem cells. *Cell* **125**, 315–326 (2006).
64. F. De Santa *et al.*, The histone H3 lysine-27 demethylase *Jmjd3* links inflammation to inhibition of polycomb-mediated gene silencing. *Cell* **130**, 1083–1094 (2007).
65. K. Nagamune, W. L. Beatty, L. D. Sibley, Artemisinin induces calcium-dependent protein secretion in the protozoan parasite *Toxoplasma gondii*. *Eukaryot. Cell* **6**, 2147–2156 (2007).
66. J. J. Thompson *et al.*, Rapid redistribution and extensive binding of NANOG and GATA6 at shared regulatory elements underlie specification of divergent cell fates. *bioRxiv [Preprint]* (2021). <https://doi.org/10.1101/2021.07.28.454132> (Accessed 25 January 2022).
67. D. Kurotaki *et al.*, Chromatin structure undergoes global and local reorganization during classical dendritic cell differentiation and activation. DNA Data Bank of Japan. <https://ddbj.nig.ac.jp/resource/bioproject/PRJDB13154>. Deposited 1 March 2022.
68. D. Kurotaki *et al.*, ChIP-seq and RNA-seq analysis during mononuclear phagocyte development. DNA Data Bank of Japan. <https://ddbj.nig.ac.jp/resource/bioproject/PRJDB3411>. Deposited 24 December 2014.
69. T. Tamura, Murine mononuclear phagocyte lineage cells. Gene Expression Omnibus. <https://www.ncbi.nlm.nih.gov/geo/query/acc.cgi?acc=GSE149762>. Deposited 20 December 2020.